Journal of Alloys and Compounds 503 (2010) 402–409

Contents lists available at ScienceDirect

Journal of Alloys and Compounds

journal homepage: www.elsevier.com/locate/jallcom

Self-propagating High-temperature Synthesis of $Ca_{1.24}Co_{1.62}O_{3.86}$ thermoelectric powders

Sidney Lin*, Jiri Selig

Dan F. Smith Department of Chemical Engineering, Lamar University, Beaumont, TX 77710, USA

ARTICLE INFO

Article history:
Received 25 April 2010
Received in revised form 1 May 2010
Accepted 3 May 2010
Available online 10 May 2010

Keywords:
Thermoelectric materials
Calcium cobaltate
Combustion synthesis
Oxide materials
Thermal analyses (TG/DSC)
X-ray diffraction (XRD)

ABSTRACT

Thermoelectric oxide, $Ca_{1.24}Co_{1.62}O_{3.86}$, was prepared by Self-propagating High-temperature Synthesis (SHS) followed by a short heat treatment. Prepared powders were characterized by XRD for phase purity. Thermal analyses (TG/DSC) were used to establish the reaction mechanism of the process and study the product thermal stability under different gas atmospheres. Temperature history of the SHS process was measured and the activation energy of the reaction was calculated from the temperature history. Electrical conductivity, thermal diffusivity, and Seebeck coefficient of the prepared power were measured.

1. Introduction

A tremendous amount of waste heat is generated from US industries (5.04×10^{18} J) and transportation (2.21×10^{19} J) [1]. The released waste heat not only reduces the fuel efficiency but also is an important factor in climate change. Thermoelectric devices provide a solution to reduce heat pollution and increase fuel efficiency at the same time. In general, thermoelectric devices are used in either electricity generation directly from a temperature difference or the creation of a temperature difference (cooling) from electricity. No moving mechanical parts are needed in these applications. The Seebeck effect describes the generation of electrical current/potential from a temperature difference (power generators) and the Peltier effect describes the creation of a temperature difference using an electrical current (solid-state coolers) [2].

A thermoelectric material is characterized by its figure of merit, *ZT*, defined by Eq. (1):

$$ZT = \frac{\alpha^2 \sigma T}{\kappa} \quad (1)$$

where α is Seebeck coefficient, σ is electrical conductivity, T is temperature, and κ is thermal conductivity.

From Eq. (1), a good thermoelectric material should have a large Seebeck coefficient, a high electrical conductivity, and a low thermal conductivity in order to maximize the *ZT* value. This implies that a viable thermoelectric compound should be both electron conductor and heat insulator at the same time. Slack suggested the best thermoelectric material would behave as a "phonon-glass/electron-crystal" (PGEC) [3]. In an ideal PGEC thermoelectric material, the thermal resistance increases due to phonons scatter at a shorter mean free path and the electrons move through the material without increasing resistance due to their longer mean free paths. It has been reported that the nanostructure inside thermoelectric materials could scatter mid- to long-wavelength phonons and thereby reduce the lattice thermal conductivity and increase the figure of merit, *ZT*.

Most of the state of the art thermoelectric materials are alloys of different metals and semiconductors, such as PbTe, SiGe, and Bi_2Te_3 because of their high electrical conductivities [4]. However, these materials have a tendency to oxidize at high temperatures and are not stable in an oxidizing atmosphere, such as inside the automobile exhaust lines where temperatures can reach as high as 800 °C. To recycle the waste heat from automobile exhaust, it is needed to develop thermoelectric materials other than alloys.

Unlike metallic and semiconducting thermoelectric materials, oxide thermoelectric materials do not oxidize or vaporize at high temperatures, retain their thermoelectric performance in oxidizing environments, and are suitable for use in severe environments, such as the exhaust line of an automobile. Several oxide materials have been reported to have good thermoelectric properties and are good

* Corresponding author at: Dan F. Smith Department of Chemical Engineering, Lamar University, 4800 MLK Blvd., Beaumont, TX 77710, USA. Tel.: +1 409 880 2314; fax: +1 409 880 2197.
E-mail address: sidney.lin@lamar.edu (S. Lin).

0925-8388/$ – see front matter © 2010 Elsevier B.V. All rights reserved.
doi:10.1016/j.jallcom.2010.05.018

candidates for automobile applications. For example, $NaCo_2O_4$ is a bronze-type compound expressed as A_xBO_2 [5] having alternating layers of CoO_2 and Na along the *c*-axis and being highly anisotropic in the *c*-axis is a good thermoelectric oxide. Single crystal $NaCo_2O_4$ [6,7] have thermoelectric properties comparable to those of Bi_2Te_3, but are difficult to produce and not economically feasible. Recently, highly textured polycrystalline $NaCo_2O_4$ samples, grown by templated grain growth (TGG) [8] and reactive templated grain growth (RTGG) [8,9] method, have shown to approach the thermoelectric properties of single crystal $NaCo_2O_4$.

Spark plasma sintering (SPS) can be used to improve thermoelectric properties of bulk oxides [10–12]. It was reported that SPS could enhance power factor and electrical conductivity. The advantage of SPS method is its rapid heat and mass transfer which results textured ceramics [12].

Complex calcium cobalt oxides were used to improve the thermoelectric performance of Na–Co–O by reducing the sodium vaporization at high temperatures [13]. Various calcium cobaltates have been reported with good thermoelectric properties, especially at high temperatures. They are good thermoelectric materials due to their layered structure, combining high mobility layers and phonon-glass layers [3]. All cobaltates have a similar structure of alternating ordered metallic CoO_2 blocks and insulating disordered blocks [14]. In the case of $Ca_{1.24}Co_{1.62}O_{3.86}$, its $[CoO_2]$ blocks are alternating with its rocksalt-type $[Ca_2CoO_3]_{0.62}$ blocks [15]. This mismatched structure leads to a reduced thermal conductivity of layered cobaltates due to a high phonon scattering at the disordered boundaries of the different building blocks [16] and provides a good combination of "phonon-glass/electron-crystal" (PGEC).

Reported processes to synthesize oxide thermoelectric powders include sol–gel or co-precipitation of metal salts followed by a high-temperature sintering, and direct solid-state sintering of mixtures of oxide, chloride, carbonate, or nitrate powders. Good *ZT* values were reported for $Ca_3Co_4O_9$ prepared by co-precipitation from metal nitrates-hydrates followed by a spark plasma sintering (SPS) [11,12], solid-state sintering followed by a solvent treatment to increase grain size [17], and $Ca_{1.24}Co_{1.62}O_{3.86}$ prepared by the precipitation method followed by templated grain growth [8]. These processes use costly or hazardous raw materials, generate hazardous gases (NO_x), acids (HCl and HNO_3), and greenhouse gas (CO_2) during the sintering. Furthermore, their long sintering periods at high temperatures make them energy intensive and increase the overall production cost.

In this work, we used a low cost solid-state combustion process, Self-propagating High-temperature Synthesis (SHS) to produce oxide thermoelectric powders. Self-propagating High-temperature Synthesis process was developed in Russia in the late 1960s and has been used to synthesize various ceramic materials, including oxides, nitrides, carbides, and metal hydrides [18,19]. In an SHS, reactants are mixed and pressed into a pellet. One end of the pellet is then ignited by an external heat source. The reaction process is highly exothermic, and reaction heat released from the combustion is sufficient to sustain the reaction front movement at room temperature. This process does not need a high-temperature furnace, and the only external heat needed is for the ignition. The fast combustion front movement (0.5–100 mm/s) enables a large-scale production in a short period of time. In addition, its fast cooling after the reaction allows the formation of metastable compounds and nanostructured ceramic powders with very fine grains that could further decrease the thermal conductivity of the products. The feasibility of a continuous SHS production of Perovskites to further reduce the production cost as well as capital investment has been proven [20]. The motivation of this work is to use the economical SHS process to produce calcium cobalt oxides with nanostructure to improve its thermoelectric performance.

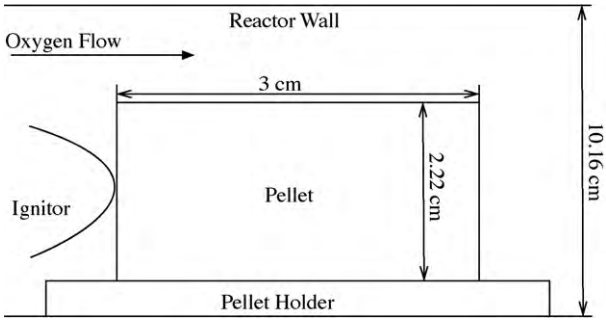

Fig. 1. Sketch of SHS reactor (not to scale).

2. Experimental

Stoichiometric proportions (Ca:Co = 1.24:1.62) of calcium peroxide powders (Alfa Aesar, 65% pure balanced with $Ca(OH)_2$), cobalt powders (Alfa Aesar, 99.5%, −325 mesh), and Co_3O_4 (Alfa Aesar, 99.7%, −400 mesh) were mechanically mixed for 4 h in a ball mill (U.S. Stoneware, Mahwah, NJ) and pressed into pellets 2.22 cm (7/8 in.) in diameter under a load of 1 metric ton. In some experiments, a solid oxidizer, $NaClO_4$ (Alfa Aesar, 98.0–102.0%, anhydrous) was used to provide additional oxygen for the synthesis. Reactant pellets were placed inside a custom made SHS reactor (Fig. 1) and ignited under an oxygen atmosphere by a graphite igniter controlled by a variable autotransformer (Staco Inc., Dayton, OH). The ignition period was about 2 s. After the ignition, the igniter was turned off and the combustion front moved forward and converted the reactants to the products as shown in reaction (2).

$$1.24CaO_2 + (1.62 - 3x)Co + xCo_3O_4 + 0.18NaClO_4 + (0.33 - 2x)O_2 \rightarrow Ca_{1.24}Co_{1.62}O_{3.86} + 0.18NaCl \quad \Delta H_r = -462\,kJ/mol\,(for\,x = 0) \tag{2}$$

In this SHS reaction scheme, cobalt metal was the fuel to provide heat needed to sustain the combustion front movement and CaO_2 served as both the solid oxidizer and the filler. The oxygen decomposed from CaO_2, and in some experiments $NaClO_4$, oxidized the adjacent cobalt powder making the reaction less dependent on the oxygen diffusing from the surrounding atmosphere. Temperature history during the SHS reaction was measured by two K-type thermocouples (Omega CHAL-020, Stamford, CT) inserted into the centerline of the pellet at a known distance apart. After the SHS reaction, products were analyzed by XRD (Bruker D8 Discover GADDS) for their phase purity.

Thermal behaviors of the reactants and products were studied using a Netzsch STA 449C TG/DSC. In all thermal analyses alumina powders were used as a reference. To understand the reaction mechanism during the SHS reaction, a loose mixture of CaO_2 and Co (Ca:Co = 1.24:1.62) was analyzed by TG/DSC under an oxygen atmosphere. Loose powders were used to minimize oxygen diffusion resistance. Oxygen, nitrogen, or air of a flow rate of 40 ml/min was used to study product stability under different atmospheres. Sample heating rate was set to be 5 or 50 °C/min. The fast heating rate (50 °C/min) was used to simulate reaction conditions of SHS conditions and the slow heating rate (5 °C/min) was used to study the thermodynamic behaviors of synthesized products.

Some SHSed powders were pressed into pellets 1/2 in. in diameter under a load of 2 metric tons and heat treated in a high-temperature furnace (Zircar Hot Spot 110) at 850 °C for different times to understand the thermal stability of the SHS products and post-treatment in some experiments.

Post-treatment on product was further studied in a tube furnace (Blue M, TF55035A) in air or oxygen. The samples were placed into the tube furnace which was preheated to 850 °C and removed immediately after the sintering to minimize possible reactions during the heating up and cooling down processes.

The thermoelectric properties of synthesized $Ca_{1.24}Co_{1.62}O_{3.86}$ powders were measured during the feasibility study at Oak Ridge National Lab. The samples were hot pressed at 850 °C under a load of 20 MPa. The Seebeck coefficient and electric resistivity were measured using ULVAC ZEM-3 system.

3. Results and discussion

3.1. TG/DSC analyses

Thermal gravity analysis of CaO_2 heated at a rate of 50 °C/min in O_2 shows two mass losses between 390 °C and 700 °C (Fig. 2). The abrupt mass loss starting from 390 °C is attributed to the decomposition of CaO_2 to form CaO and O_2. This decomposition is endothermic as indicated by a negative DSC peak. The endothermic peak reaches a minimum at 425 °C. The mass loss caused by

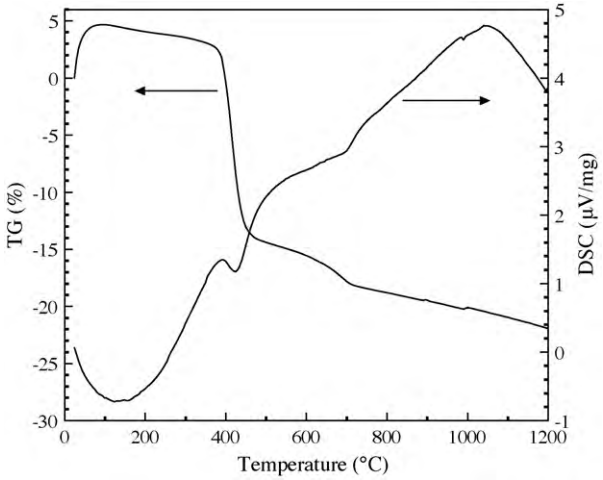

Fig. 2. TG/DSC of CaO_2 in oxygen heated at a rate of 50 °C/min.

decomposition of CaO_2 is 15%, which agrees for sample initially containing 65% CaO_2 and 35% of $Ca(OH)_2$ as reported by the manufacturer. Another noticeable drop in the TG measurement occurs at 702 °C indicates the decomposition of $Ca(OH)_2$ to form CaO and water. Again, this decomposition is endothermic with a negative DSC slope change. Reactions (3) and (4) show the decompositions of the CaO_2 and $Ca(OH)_2$ in O_2 during the SHS reaction.

$$CaO_2 \rightarrow CaO + (1/2)O_2 \quad (425\,^{\circ}C) \tag{3}$$

$$Ca(OH)_2 \rightarrow CaO + H_2O \quad (702\,^{\circ}C) \tag{4}$$

Sodium perchlorate which is used as a solid oxidizer in some experiments decomposes exothermically to oxygen and sodium chloride at 594 °C when heated at 50 °C/min in O_2 (Fig. 3). Before decomposition, $NaClO_4$ melts as indicated by the endothermic peak at 504 °C. Sodium chloride melts at 832 °C and begins to vaporize at 950 °C. Vaporization of NaCl is complete at 1180 °C. Because NaCl vaporize at a relatively low temperature the final product of SHS reaction should be NaCl free. Any leftover NaCl can be easily washed away by warm DI water. Reactions (5)–(7) show the decomposition of $NaClO_4$ during the SHS reaction and subsequent melting and evaporation of NaCl.

$$NaClO_4 \rightarrow NaCl + 2O_2 \quad (594\,^{\circ}C) \tag{5}$$

$$NaCl_{(s)} \rightarrow NaCl_{(l)} \quad (832\,^{\circ}C) \tag{6}$$

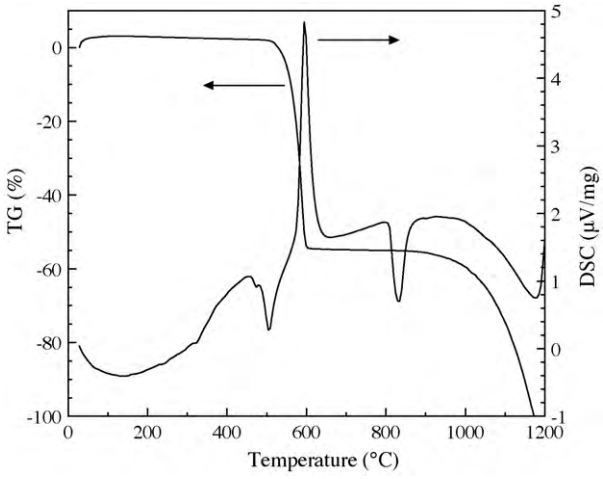

Fig. 3. TG/DSC of $NaClO_4$ in oxygen heated at a rate of 50 °C/min.

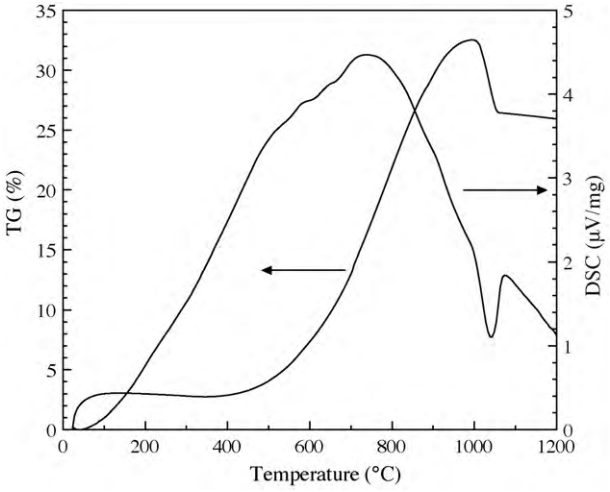

Fig. 4. TG/DSC of Co in oxygen heated at a rate of 50 °C/min.

$$NaCl_{(l)} \rightarrow NaCl_{(g)} \quad (\geq 950\,^{\circ}C) \tag{7}$$

TG curve for cobalt metal heated at a rate of 50 °C/min in O_2 (Fig. 4) shows oxidation between 450 °C and 998 °C followed by a decomposition. Several small peaks on DSC curve between 450 °C and 998 °C suggest that the oxidation of Co to Co_3O_4 is a multiple step reaction. The first exothermic peak on DSC curve is observed at 520 °C and corresponds to the formation of CoO and second peak is observed at 620 °C and corresponds to the formation of Co_3O_4. The mass gain during the oxidation was approximately 33% which is in agreement with complete oxidation of cobalt to Co_3O_4. After oxidation, a sudden drop in mass is observed above 1000 °C. This drop is concurrent with a large endothermic peak on DSC curve at 1038 °C. This mass drop is 8%, which represents decomposition of Co_3O_4 to CoO and oxygen. Oxidation of cobalt and its subsequent decomposition can be expressed in series of three reactions (8)–(10).

$$Co + (1/2)O_2 \rightarrow CoO \quad (450\text{–}520\,^{\circ}C) \tag{8}$$

$$CoO + (1/6)O_2 \rightarrow (1/3)Co_3O_4 \quad (520\text{–}998\,^{\circ}C) \tag{9}$$

$$(1/3)Co_3O_4 \rightarrow CoO + (1/6)O_2 \quad (1038\,^{\circ}C) \tag{10}$$

From reactions (3) and (5), it is clear that the oxygen from the decomposed CaO_2 and $NaClO_4$ can be used for oxidization of Co metal immediately as designed for this SHS reaction. Because of the oxygen from decomposition has a higher temperature than that from the surrounding gas phase it increases the SHS reaction rate.

For sample containing mixture of reactants heated at 50 °C/min three main reaction steps are observed during the analysis (Fig. 5). The first step is the decomposition of CaO_2 to CaO and O_2 between 384 °C and 460 °C which is similar to the thermal behavior of CaO_2 alone (Fig. 2). The second step is Co oxidation and subsequent $Ca_{1.24}Co_{1.62}O_{3.86}$ formation, between 460 °C and 988 °C. It is clear that cobalt oxidation starts at a lower temperature when CaO_2 is present, which proves CaO_2 is acting as an oxidizer as well as filler in our reaction. A sudden slope change of TG curve around 690 °C which is the same $Ca(OH)_2$ decomposition observed in Fig. 5. However, no net weight loss was detected. The DSC curve reaches a maximum at 754 °C and the slope of TG curve slowly decreases after that temperature. This suggests that the reaction slows down once the temperature is lower than 754 °C. The last major step is the decomposition of the $Ca_{1.24}Co_{1.62}O_{3.86}/Co_3O_4$ mixture beginning at 998 °C to form CaO, CoO and O_2. Sample is fully decomposed at 1035 °C. The endothermic decomposition is indicated by a negative DSC peak at 1015 °C.

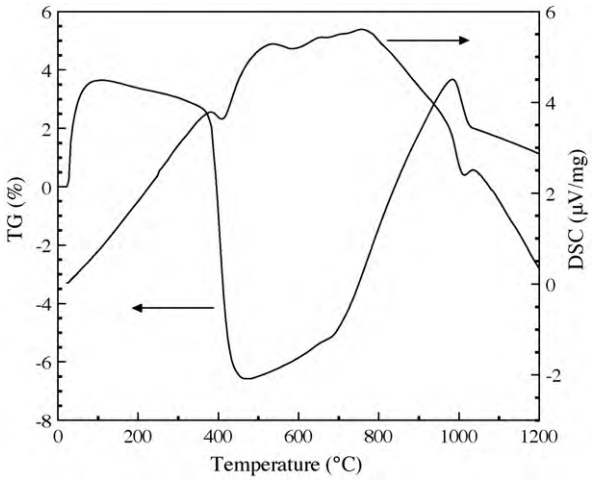

Fig. 5. TG/DSC of a mixture of CaO_2 and Co (Ca:Co = 1.24:1.62) in oxygen heated at a rate of 50 °C/min.

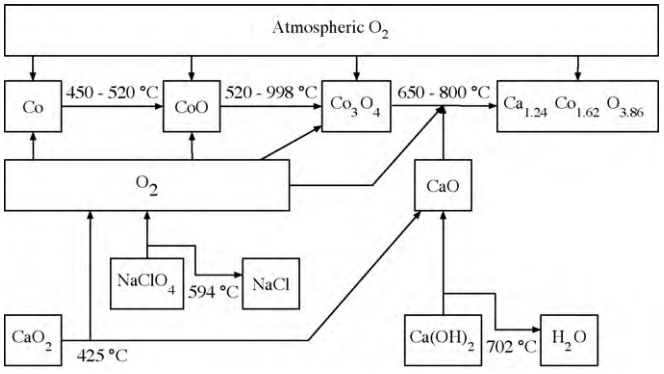

Fig. 7. Proposed reaction mechanism of $1.24CaO_2 + (1.62 - 3x)Co + xCo_3O_4 + 0.18NaClO_4 + (0.33 - 2x)O_2 \rightarrow Ca_{1.24}Co_{1.62}O_{3.86}$.

If reaction (2) reaches a 100% conversion a 10% increase in mass should be observed. However, our TG results in Fig. 5 show a significantly less mass increase which suggests the conversion of reactants to $Ca_{1.24}Co_{1.62}O_{3.86}$ is not complete during the thermal analyses. The product at the highest conversion (highest mass of the TG curve) at 998 °C is most likely a mixture of $Ca_{1.24}Co_{1.62}O_{3.86}$, CaO, and Co_3O_4. Oxidation of cobalt metal and formation of $Ca_{1.24}Co_{1.62}O_{3.86}$ can be confirmed by the decomposition at 998 °C (mass decrease in the TG curve). Similar decomposition of $Ca_{1.24}Co_{1.62}O_{3.86}$ was reported at 956 °C [13]. However, because the decompositions of calcium cobalt oxide and Co_3O_4 occur at close temperature ranges it is not clear from the TG/DSC results how much of Co_3O_4 or $Ca_{1.24}Co_{1.62}O_{3.86}$ is present at 998 °C before the decompositions take place.

Fig. 6 shows the TG/DSC results when different heat rates were used in analyzing the reactant mixture. It can be seen when a faster heating rate (50 °C/min) was used, the reaction temperature of each step shifted to a higher temperature due to the larger temperature gradient inside the sample as predicted by Kissinger [21]. In addition, a slower heating rate (5 °C/min) results lower amplitude of peaks on DSC curve (Fig. 6a) and decreases temperature ranges for phase transitions and reactions by approximately 25 °C. A significant difference in TG results is also observed (Fig. 6b). There is a larger mass increase between 450 °C and 950 °C when the sample was heated at 5 °C/min which suggests more product is formed during the slow heating analysis.

TG/DSC analysis suggests that during the SHS reaction, six major reaction steps occur. The reaction mechanism of reaction (2) is proposed in Fig. 7. The SHS reaction starts with the decomposition of calcium peroxide to form calcium oxide and oxygen at 425 °C. At the same time, cobalt metal begins to oxidize at 450 °C which results in large amount of heat release. The oxidation of cobalt is the main reaction that results in reaction front propagation. Oxidation of cobalt occurs in two steps – formation of CoO at 520 °C followed by the formation of Ca_3O_4 at 620 °C. As Co_3O_4 is formed it reacts with calcium oxide to form $Ca_{1.24}Co_{1.62}O_{3.86}$. When temperature reaches 594 °C sodium perchlorate decomposes to sodium chloride and oxygen which accelerates the oxidation of cobalt. At 702 °C calcium hydroxide decomposes to water and forms additional calcium oxide which also reacts with Co_3O_4. If a too high temperature is reached during SHS reaction $Ca_{1.24}Co_{1.62}O_{3.86}$ may decompose back to CoO and CaO. The dominant reaction steps for $Ca_{1.24}Co_{1.62}O_{3.86}$ formation are summarized in Table 1.

3.2. SHS of $Ca_{1.24}Co_{1.62}O_{3.86}$

The thermodynamic properties [22] of reactants and products of reaction (2) were listed in Table 2 to calculate the reaction heat and the adiabatic temperature. Eq. (11) was used to calculate the

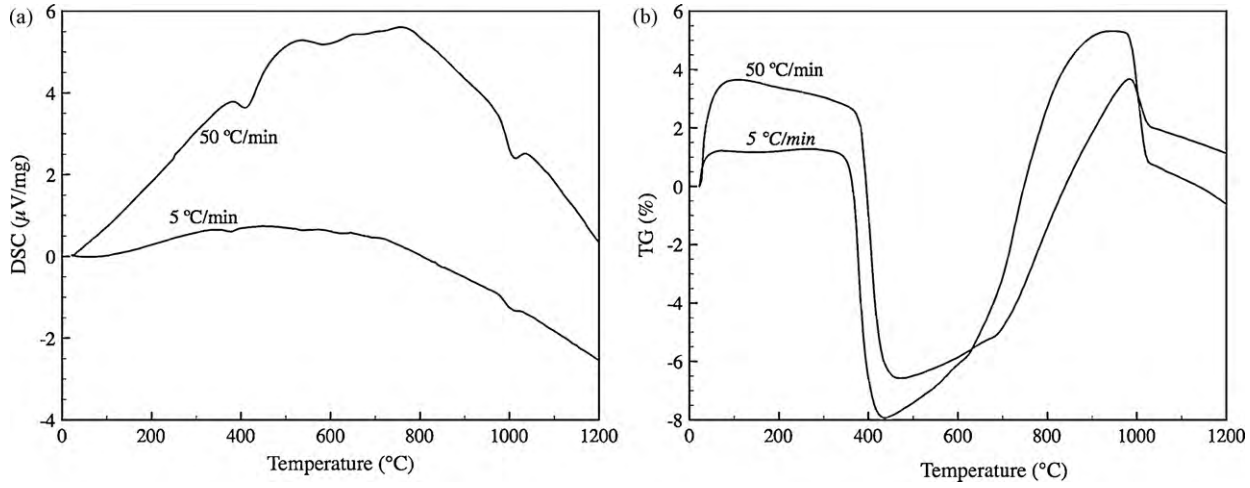

Fig. 6. TG of a mixture of CaO_2 and Co (Ca:Co = 1.24:1.62) in oxygen (a) heated at a rate of 5 °C/min and (b) heated at a rate of 50 °C/min.

Table 1
Summary of reaction steps during SHS of $Ca_{1.24}Co_{1.62}O_{3.86}$.

Reactions	ΔH (kJ/mol)	Temperature range (°C)
$1.24CaO_2 \rightarrow 1.24CaO + 0.62O_2$ (65%)	19.9	384–460
$1.24Ca(OH)_2 \rightarrow 1.24CaO + 1.24H_2O$ (35%)	92.3	690–702
$0.18NaClO_4 \rightarrow 0.09O_2 + 0.18NaCl$	−28.4	594
$1.62Co + 0.81O_2 \rightarrow 1.62CoO$	−237.7	450–520
$1.62CoO + 0.27O_2 \rightarrow 0.54Co_3O_4$	−177.9	520–998
$1.24CaO + 1.62Co_3O_4 + 0.23O_2 \rightarrow Ca_{1.24}Co_{1.62}O_{3.86}$	−456.5	650–800 [14]
$Ca_{1.24}Co_{1.62}O_{3.86} \rightarrow 1.24CaO + 1.62Co_3O_4 + 0.23O_2$		≥998
$1.62Co_2O_3 \rightarrow 1.62Co + 0.27O_2$		≥1038

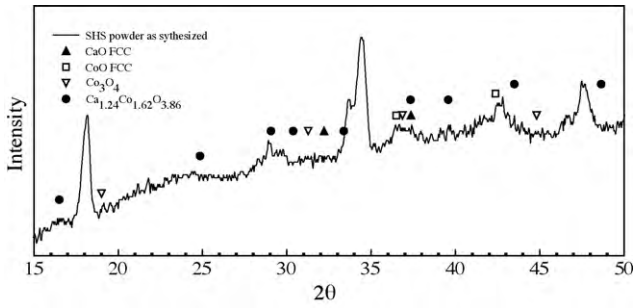

Fig. 8. XRD pattern of product of SHS reaction. Reference peaks for $Ca_{1.24}Co_{1.62}O_{3.86}$ are taken from Itahara and Tani [8].

adiabatic temperature.

$$\int_{298}^{T_{ad}} \left(\sum_i n_i C_{pi} \right) \, dT = -\Delta H_r \tag{11}$$

In this equation n_i and C_{pi} are the stoichiometric coefficient and specific heat of product ($Ca_{1.24}Co_{1.62}O_{3.86}$ and NaCl). To simplify the calculation a heat capacity of $Ca_{1.24}Co_{1.62}O_{3.86}$ (220 J/mol K) estimated from that of CaO and Co_3O_4 and specific heat of NaCl at 1500 K are used. Values of specific heats are in Table 2. The calculated adiabatic temperature is 2265 K.

Ignition of the sample occurs in about 2 s after the igniter is turned on. Reaction front propagates through the pellet from the ignition region towards the unreacted remainder of the pellet. Sometimes, a pulsating reaction front movement is observed. Pulsating reaction front often indicates reaction instability or the reaction front movement is barely self-sustainable. If $NaClO_4$ solid oxidizer is used a white smoke (vaporized NaCl) is observed during the reaction. After the reaction front propagates through the whole pellet, the center part of sample glows for several minutes before slowly cools down. During the SHS reaction, the color of the pellet changes from light grey to dark grey. Synthesized sample is porous and easy to grind. As-synthesized samples were analyzed by XRD to identify their phases (Fig. 8). No detectable amount of unreacted reactants nor cobalt oxides or calcium oxide is found by XRD in the product. The XRD pattern shows unidentified peaks which are believed to be calcium cobalt oxide of unknown stoichiometry or $Ca_{1.24}Co_{1.62}O_{3.86}$ intermediate compounds of a different lattice constant or structure than the reported one [8].

Table 2
Heats of formation and heat capacities of reactants and products in the proposed SHS reaction.

Compound	ΔH_f (kJ/mol)	C_p (J/mol K)
Co	0	
CaO_2	−654.8	
$NaClO_4$	−382.6	
CaO	−382.6	56
Ca_3O_4	−382.6	228
$Ca_{1.24}Co_{1.62}O_{3.86}$	−1268.4 (estimated)	220 (estimated)
NaCl	−411.1	75

Fig. 9 shows the temperature history at the centerline of the reaction pellet during the SHS process (reaction (2)). The temperature increases from room temperature to 1200 °C in 65 s and then cools down below 650 °C (the minimum temperature for $Ca_{1.24}Co_{1.62}O_{3.86}$ formation) in 200 s. As seen from the TG/DSC analyses in Fig. 6, even at a much slower heating rate (5 °C/min), the reactants do not have enough time to form the desired product completely before temperature reaches the decomposition temperature of $Ca_{1.24}Co_{1.62}O_{3.86}$ (1038 °C). The maximum temperature reached during the SHS is 1200 °C, which is 160 °C higher than the decomposition of $Ca_{1.24}Co_{1.62}O_{3.86}$. However, the duration of temperature above the decomposition temperature is only 60 s, which is not sufficient for $Ca_{1.24}Co_{1.62}O_{3.86}$ to decompose completely but instead a mixture of undesired Ca–Co–O may be formed. A temperature plateau at 1175 °C lasting for 20 s in Fig. 9 is caused by the vaporization of sodium from $NaClO_4$ decomposition.

3.3. Post-treatment of SHS products

In our previous work [23], it has been found that SHSed powder can be converted to $Ca_{1.24}Co_{1.62}O_{3.86}$ by sintering at 850 °C for 2 h in air. This suggests that the product obtained after SHS is a kinetically preferred metastable compound and can be converted to a thermodynamically preferred product ($Ca_{1.24}Co_{1.62}O_{3.86}$) by sintering at a temperature lower than its decomposition temperature. During the SHS, reaction pellet heats up rapidly to almost 1200 °C and it takes approximately 5 min for the sample to cool down below 450 °C (Fig. 9). No reaction should occur bellow 450 °C according to TG/DSC analyses. This fast heating and cooling processes may not enable the sample to achieve the thermodynamically preferred state but some metastable compound is formed.

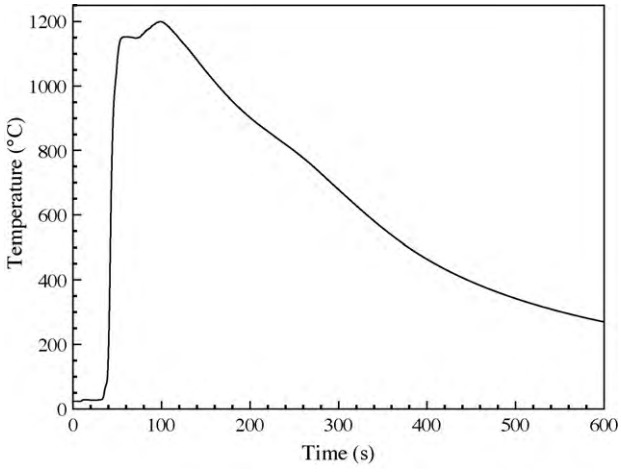

Fig. 9. Temperature history of SHS reaction at the center of reactant pellet.

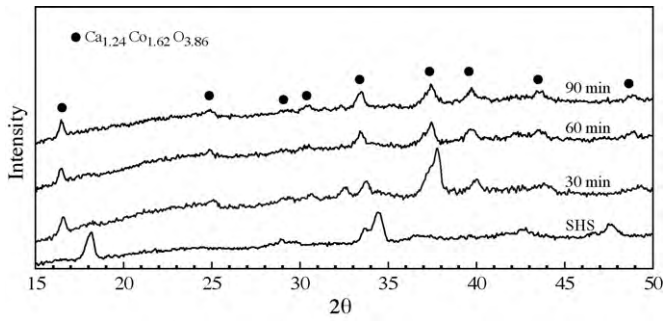

Fig. 10. XRD patterns of SHS powder (a) as-synthesized, (b) sintered at 850 °C for 30 min in O_2, (c) sintered at 850 °C for 60 min in O_2, and (d) sintered at 850 °C for 90 min in O_2. Reference peaks for $Ca_{1.24}Co_{1.62}O_{3.86}$ are taken from Itahara and Tani [8].

To understand and improve the post-treatment process, samples were heated in a tube furnace in an oxygen or air atmosphere to study the impact of sintering time on the final product. Fig. 10 shows XRD patterns of samples post-treated in a tube furnace for various time periods at 850 °C in oxygen. It can be seen from Fig. 10b that after sintering at 850 °C in oxygen for 30 min, desired product ($Ca_{1.24}Co_{1.62}O_{3.86}$) starts to form, although there is an unidentified XRD peak at $2\theta = 32.5°$. Samples sintered for 60 and 90 min in the same condition have the same XRD patterns and contain only $Ca_{1.24}Co_{1.62}O_{3.86}$ (Fig. 10c and d). It can be concluded that highly pure $Ca_{1.24}Co_{1.62}O_{3.86}$ can be obtained by a 1 h post-treatment at 850 °C in oxygen.

X-ray diffraction of as-synthesized products post-treated in a tube furnace at 850 °C in air shows that a 15-min post-treatment in air can produce pure $Ca_{1.24}Co_{1.62}O_{3.86}$ (Fig. 11b). There is no change in composition when post-treatment time is increased to 30 and 60 min (Fig. 10c and d). These results suggest that powders obtained from our SHS are very good precursor for bulk thermoelectric devices and can be easily converted to pure $Ca_{1.24}Co_{1.62}O_{3.86}$ during a hot pressing process.

3.4. Thermal stability of $Ca_{1.24}Co_{1.62}O_{3.86}$ synthesized by SHS

TG analysis was conducted to study the thermal stability of the product. Fig. 12 shows the results of TG curves of pure $Ca_{1.24}Co_{1.62}O_{3.86}$ (SHS followed by a 10 h 850 °C post-treatment) in N_2, O_2, and air separately. Samples were placed above a thin layer of alumina to prevent possible reaction between the product and sample crucible. When a high enough temperature (at least 900 °C, depending on atmosphere) is reached, $Ca_{1.24}Co_{1.62}O_{3.86}$ decomposes to CaO, CoO, and O_2. The release of oxygen results is 7.7% mass loss.

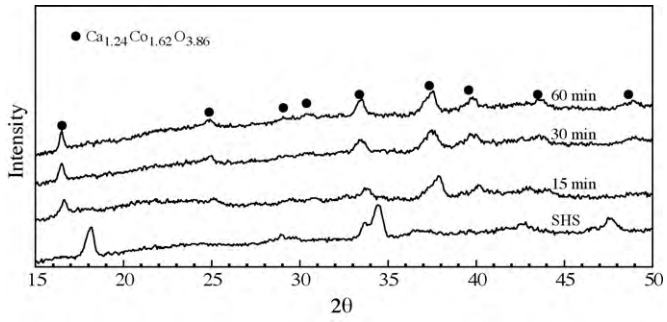

Fig. 11. XRD patterns of SHS powder (a) as-synthesized, (b) sintered at 850 °C for 15 min in air, (c) sintered at 850 °C for 30 min in air, and (d) sintered at 850 °C for 60 min in air. Reference peaks for $Ca_{1.24}Co_{1.62}O_{3.86}$ are taken from Itahara and Tani [8].

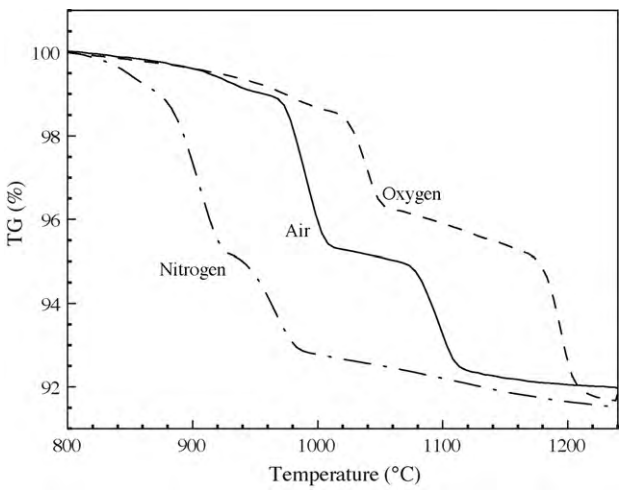

Fig. 12. TG curves of $Ca_{1.24}Co_{1.62}O_{3.86}$ heated at a rate of 10 °C/min (a) Al_2O_3 blank, (b) in N_2, (c) in air, and (d) in O_2.

For sample analyzed in N_2 the mass decreases 7% of its initial mass between 850 °C and 1000 °C indicates the decomposition of $Ca_{1.24}Co_{1.62}O_{3.86}$ to CaO, CoO, and O_2. The decomposition of $Ca_{1.24}Co_{1.62}O_{3.86}$ occurs in two steps with first step starting at 850 °C and second step beginning at 920 °C and finishing at 1000 °C. Similar decomposition in air and oxygen atmospheres occurs between 950 °C and 1100 °C and between 1020 °C and 1200 °C respectively. These results suggest that the decomposition temperature and thus the stability of $Ca_{1.24}Co_{1.62}O_{3.86}$ is increased with increasing amount of partial pressure of oxygen.

3.5. Activation energy

Activation energy of the SHS reaction can be calculated from the maximum temperatures and the velocities of the reaction front movement when different amounts of diluent are added to the SHS reaction system using the equation below [24,25]:

$$u = k \exp\left(\frac{-E}{2RT}\right) \tag{12}$$

where u is reaction front propagation speed, k is a pre-exponent, E is the activation energy, R is the gas constant, and T is the maximum combustion temperature reached during SHS reaction. The maximum combustion temperature and the reaction front movement velocity can be calculated from the temperature history measured at two points on the centerline of the reaction pellet. Activation energy is calculated from the slope of the straight line in the Arrhenius plot. Fig. 13 is the Arrhenius plot of reaction front movement and maximum combustion temperature for $x = 0$, 0.025, 0.05, and 0.075 dilution is used. From Fig. 13, the activation of reaction (2) is calculated to be 71 kJ/mol.

3.6. Thermoelectric properties

SHS powders followed by a 15 min post-treatment were hot pressed and analyzed for their thermoelectric properties in a temperature range of 25–500 °C. Fig. 14 shows the Seebeck coefficients of our sample. SHS sample has an almost constant Seebeck coefficient of 165 μV/K in this temperature range which is higher than the reported data of samples prepared by other processes including conventional solid-state sintering (CS) [14] and spark plasma sintering (SPS) [14,15]. However, the electrical conductivity of our sample is lower than those prepared by spark plasma sintering but higher than the reported data from solid-state sintering (Fig. 15).

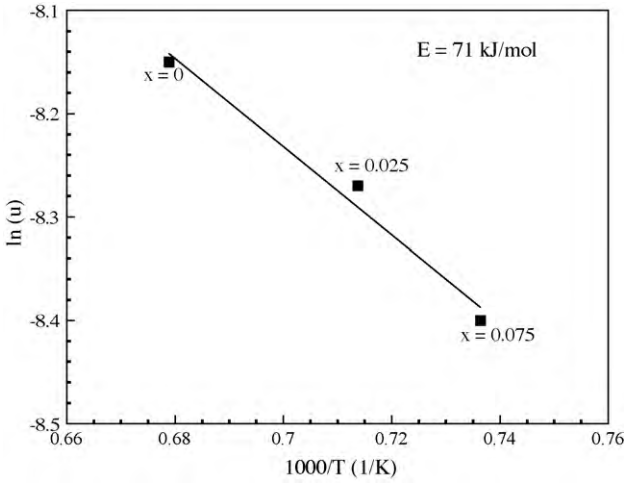

Fig. 13. Arrhenius plot of experimental data used to calculate activation energy of SHS of $Ca_{1.24}Co_{1.62}O_{3.86}$.

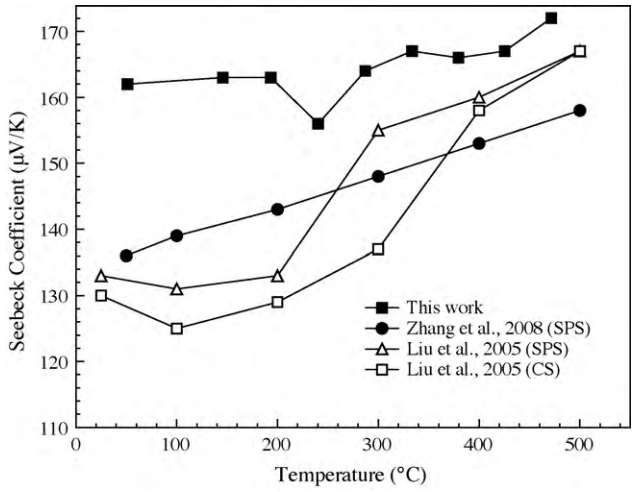

Fig. 14. Seebeck coefficient compared with $Ca_3Co_4O_9$ prepared by different methods [11,12].

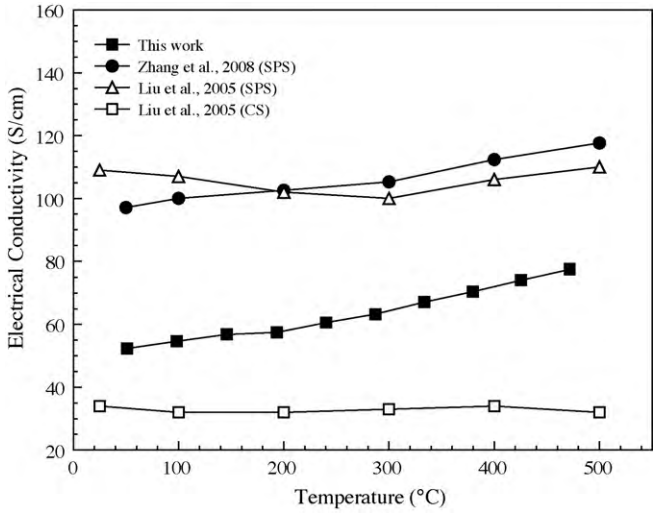

Fig. 15. Electrical conductivity compared with $Ca_3Co_4O_9$ prepared by different methods [11,12].

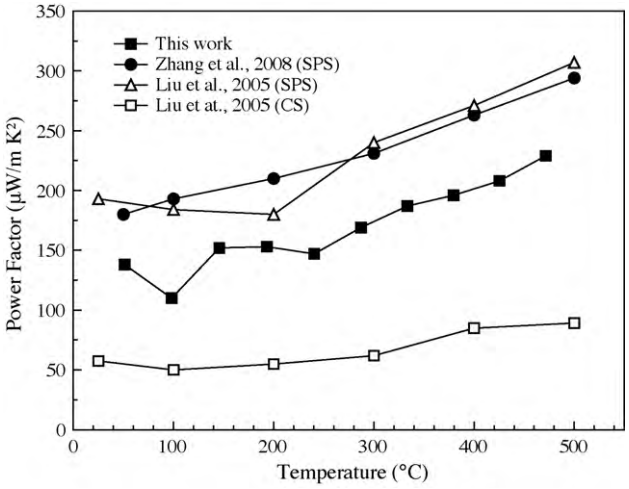

Fig. 16. Power factor compared with $Ca_3Co_4O_9$ prepared by different methods [11,12].

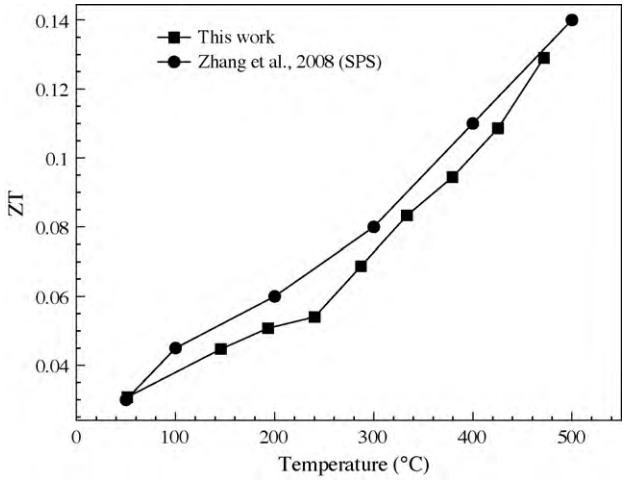

Fig. 17. *ZT* values compared with $Ca_3Co_4O_9$ prepared by different methods [12].

Because of the lower thermal conductivity, the thermal power of our sample is also lower than those prepared by spark plasma sintering process (Fig. 16). The room temperature thermal diffusivity of our sample (0.0088 cm^2/s) is used to calculate the figure of merit. From Fig. 17, it can be seen that SHS powders consolidated by hot press has figure of merit close to samples prepared by spark plasma sintering process.

4. Conclusion

In this work $Ca_{1.24}Co_{1.62}O_{3.86}$ was successfully synthesized by SHS followed by a short post-treatment at 850 °C. Powders obtained from SHS reaction contain an unidentified intermediate compound and can be easily converted to $Ca_{1.24}Co_{1.62}O_{3.86}$ by a 15 min post-treatment in air. The hot pressed SHS powders have a high Seebeck coefficient and a figure of merit close to samples prepared by spark plasma sintering process. Thermal analyses (TG/DSC) were used to study the reaction network. TG/DSC analysis of pure $Ca_{1.24}Co_{1.62}O_{3.86}$ suggests that the decomposition temperature increases with oxygen partial pressure. Temperature history and velocity of combustion front movement were measured. The activation energy of the SHS reaction is calculated to be 75 kJ/mol.

Acknowledgements

This work was partially supported by Lamar University Research Enhancement Grants under project no. CM1006 and Texas Hazardous Waste Research Center (THWRC) under contract no. 068LUB0969. The authors would like to express their special thank to Dr. Hua-Tay Lin and Dr. Hsin Wang of the Oak Ridge National Laboratory for measuring the thermoelectric properties during the feasibility test. The authors also wish to thank Dr. Andrew Gomes, Mr. Doanh Tran, and Ms. Lauren Griffin for assistance in sample analyses and helpful discussion.

References

[1] U.S. Energy Flowchart 2008, Lawrence Livermore National Laboratory. https://publicaffairs.llnl.gov/news/energy/energy.html.
[2] D.M. Rowe (Ed.), CRC Handbook of Thermoelectrics, CRC Press LLC, Boca Raton, FL, 1995.
[3] G.A. Slack, in: D.M. Rowe (Ed.), CRC Handbook of Thermoelectrics, CRC Press, Boca Raton, FL, 1995, p. 407.
[4] G.J. Snyder, E.S. Toberer, Nat. Mater. 7 (2008) 105–114.
[5] R. Ray, A. Ghoshray, K. Ghoshray, S. Nakamura, Phys. Stat. Sol. (b) 215 (1999) 703–707.
[6] G. Mahan, Proceeding of Int. Conference on Thermoelectrics, Dresden, Germany, 1997.
[7] G. Peleckis, T. Motohashi, M. Karppinen, H. Yamauchi, Appl. Phys. Lett. 83 (2003) 5416.
[8] H. Itahara, T. Tani, R&D Rev. Toyota CRDL 39 (2004) 63–70.
[9] S. Tajima, T. Tani, S. Isobe, K. Koumoto, Mater. Sci. Eng. B 86 (2001) 20–25.
[10] A. Kikuch, L. Zhang, N. Okinaka, T. Tosho, T. Akiyama, Mater. Trans. 50 (2009) 2675–2679.
[11] Y. Liu, Y. Lin, Z. Shi, C. Nan, Z. Shen, J. Am. Ceram. Soc. 88 (2005) 1337–1340.
[12] Y. Zhang, J. Zhang, J. Mater. Process. Technol. 208 (2008) 70–74.
[13] S. Li, R. Funahashi, I. Matsubara, K. Ueno, H. Yamada, J. Mater. Chem. 9 (1999) 1659–1660.
[14] A.C. Masset, C. Michel, A. Maignan, M. Hervieu, O. Toulemonde, F. Studer, B. Raveau, J. Hejtmanek, Phys. Rev. B 62 (2000) 167–175.
[15] J. Sugiyama, A. Mystery in Thermoelectric Layered Cobaltites, R&D Rev. Toyota CRDL 39 (2004) 50–62.
[16] Q. Li, Mater. Res. Soc. Symp. Proc. 886 (2006), 0886-F01-05.1–0886-F01-05.12.
[17] M. Mikami, E. Guilmeau, R. Funahashi, K. Chong, D. Chateigner, J. Mater. Res. 20 (2005) 2492–2497.
[18] A.S. Mukasyan, K.S. Martirosyan, Combustion of Heterogeneous Systems: Fundamentals and Applications for Materials Synthesis, Transworld Research Network, Kerala, India, 2007.
[19] A. Varma, G. Cao, M. Morbidelli, AIChE J. 36 (1990) 1032–1038.
[20] S.C. Lin, J.T. Richardson, D. Luss, Physica C 260 (1996) 321–326.
[21] H.E. Kissinger, Anal. Chem. 29 (1957) 1702–1706.
[22] C.L. Yaws, Yaws' Handbook of Thermodynamic Properties for Hydrocarbons and Chemicals. Knovel. http://knovel.com/web/portal/browse/display?_EXT_KNOVEL_DISPLAY_bookid=2380&VerticalID=0.
[23] S. Lin, J. Selig, J.A. Gomes, and D. Tran, The Materials Science & Technology 2009 Conference and Exhibition proceedings (2009) 241-252, ISBN 13: 978-1-61503r-r006-4.
[24] A.B. Zeldovich, The Mathematical Theory of Combustion and Explosions, Consultants Bureau, New York, NY, 1985 (translated from Russian).
[25] K.K. Kuo, Fundamentals of Solid-Propellant Combustion, American Institute of Aeronautics and Astronautics, New York, NY, 1984.